Supporting Information

Quantification of charge compensation in lithium- and manganese-rich Li-ion cathode materials by X-ray spectroscopy

Shehab E. Ali[1,2], Wojciech Olszewski[1,3], Carlo Marini[1], Arefeh Kazzazi[4,5], Hyeongseon Choi[4,5], Matthias Kuenzel[4,5], Dominic Bresser[4,5], Stefano Passerini[4,5], Dino Tonti[6,*], Laura Simonelli[1,*]

[1] *ALBA Synchrotron Light Facility, Carrer de la Llum 2-26, 08290 Cerdanyola del Vallès, Spain*

[2] *Physics Department, Faculty of Science, Suez Canal University, Ismailia, Egypt*

[3] *Faculty of Physics, University of Bialystok, ul. K. Ciolkowskiego 1L, 15-245 Bialystok, Poland*

[4] *Helmholtz Institute Ulm (HIU), Helmholtzstrasse 11, 89081 Ulm, Germany*

[5] *Karlsruhe Institute of Technology (KIT), PO Box 3640, 76021 Karlsruhe, Germany*

[6] *Inst. de Ciència de Materials de Barcelona, Consejo Superior de Investigaciones Cientìficas, Campus UAB Bellaterra, Spain*

***Corresponding authors:** lsimonelli@cells.es; dtonti@icmab.es

Electrochemical data

The charge points along the voltage profiles during the first cycle of $Li[Li_{0.2}Ni_{0.16}Mn_{0.56}Co_{0.08}]O_2$ were defined via the specific capacity: P01 corresponds to the pristine electrode, P03 corresponds to a specific capacity of 100 mAh g^{-1}, P04 to 200 mAh g^{-1}, and P08 indicates the fully charged (to 4.8 V) and subsequently discharged (to 2.5 V) sample (see **Figure S1a,b**). Since the current-induced polarization affects the shape of the voltage profile (see **Figure S1a**), we normalized the voltage profiles obtained at higher dis-/charge rates (1C and 5C) to the one obtained at 0.1C in order to estimate the effect of, e.g., side reactions with the electrolyte at elevated potentials. In the absence of such side effects, one would expect the normalized voltage profiles to overlap with those obtained at low rates, which is indeed the case for P03, i.e., 100 mAh g^{-1} (**Figure S1c**). For P04, however, this is not the case anymore, as in this case very high overpotentials lead to accelerated side reactions with the electrolyte, and a significant amount of the capacity recorded originates from electrolyte decomposition. In order to also take this into account and better estimate the true charge capacity of the active material, we compressed the x axis in such a way that the curves coincide again (**Figure S1d**). From these curves, we were able to estimate the true charge capacity of the active material at P04, which is roughly 170 mAh g^{-1} for the electrode charged at 1C and about 160 mA h g^{-1} for that charged at 5C.

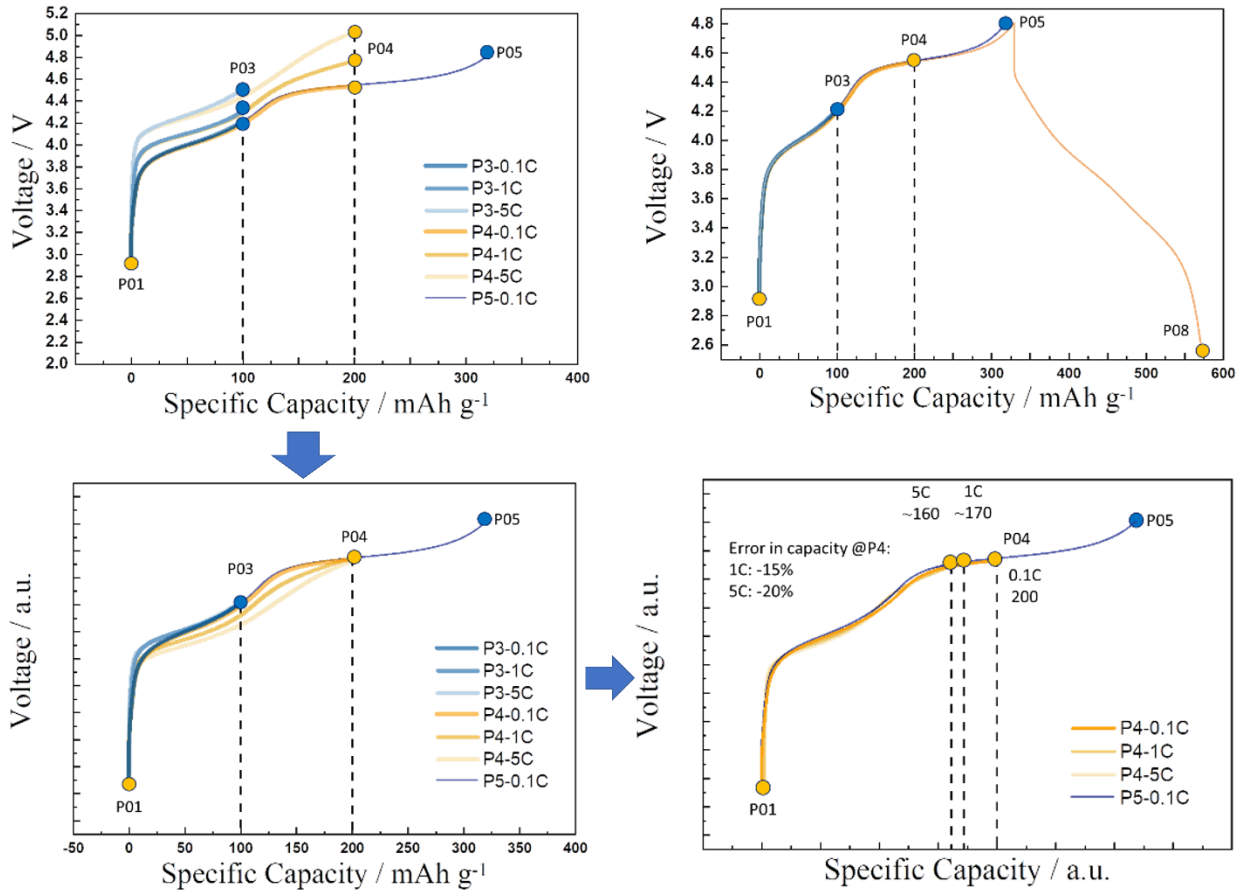

Figure S1. (a) Voltage profiles of $Li[Li_{0.2}Ni_{0.16}Mn_{0.56}Co_{0.08}]O_2$ electrodes cycled in half-cell configuration, where the points P01 (pristine), P03 and P04 (beginning and end of the voltage plateau), P05 (fully charged) have been indicated for all samples. (b) All points obtained for the sample dis-/charged at 0.1C, including P08 for the complete charge-discharge cycle. (c) Voltage profiles normalized, considering the current-induced overpotential. (d) Estimated "true" charge capacity of the active material at elevated charge rates up to P04 after subtracting the estimated contribution from side reactions such as electrolyte decomposition at elevated potentials owing to the higher charge rate.

EXAFS analysis

The present study mainly focuses on the first charge and discharge cycle, at a few representative charge points: the pristine state (P01), the beginning (P03) and the end (P04) of the high voltage plateau, and the fully charged (P05) and following discharged state (P08). The Mn, Co, and Ni K-edge EXAFS oscillations measured at several temperatures and the corresponding Fourier transforms (FTs) of the EXAFS signal, providing real-space information on the partial atomic distribution around the Mn, Co and Ni atoms, are reported in **Figure S2**.

The Mn, Co, and Ni K-edge EXAFS signals are multiplied by k^2 to enhance the signal in the higher k region. The FTs are performed over the k range 2.6–15.8 $Å^{-1}$ for Mn, 2.5-12.3 $Å^{-1}$ for Co, and 3.6-11.8 $Å^{-1}$ for Ni. In **Figure S2d**, the main peaks at ~1.44 Å and ~2.42 Å correspond to single scattering contributions from the nearest neighbor O atoms and the next-nearest neighbor transition metal (TM = Mn, Co, Ni) atoms around Mn, respectively. The peaks at ~1.5 Å and ~2.4 Å shown in **Figure S2e** correspond to the first and second coordination shell around Co composed by O and (TM = Mn, Co, Ni) atoms, respectively. **Figure S2f** shows the FTs peaks at ~1.58 Å and 2.58 Å corresponding to the first and second coordination shell composed of O and TM (Mn, Co, Ni) atoms, respectively, around Ni.

For the quantification of the local structure, the EXAFS oscillations were modeled using the general equation assuming the single-scattering approximation:

$$\chi(k) = \sum_i \frac{N_i S_0^2}{kR_i^2} f_i(k, R_i) e^{\frac{-2R_i}{\lambda}} e^{-2k^2\sigma_i^2} \sin[2kR_i + \delta_i(k)] \qquad (1)$$

where N_i is the number of neighboring atoms at a distance R_i from the absorbing atom, S_0^2 is the passive electron reduction factor, $f_i(k, R_i)$ is the backscattering amplitude, λ is the photoelectron mean free path, $\delta_i(k)$ is the phase shift, and σ_i^2 is the Debye-Waller factor (DWF) measuring the mean square relative displacements (MSRDs) of the photo-absorber backscatter pairs.

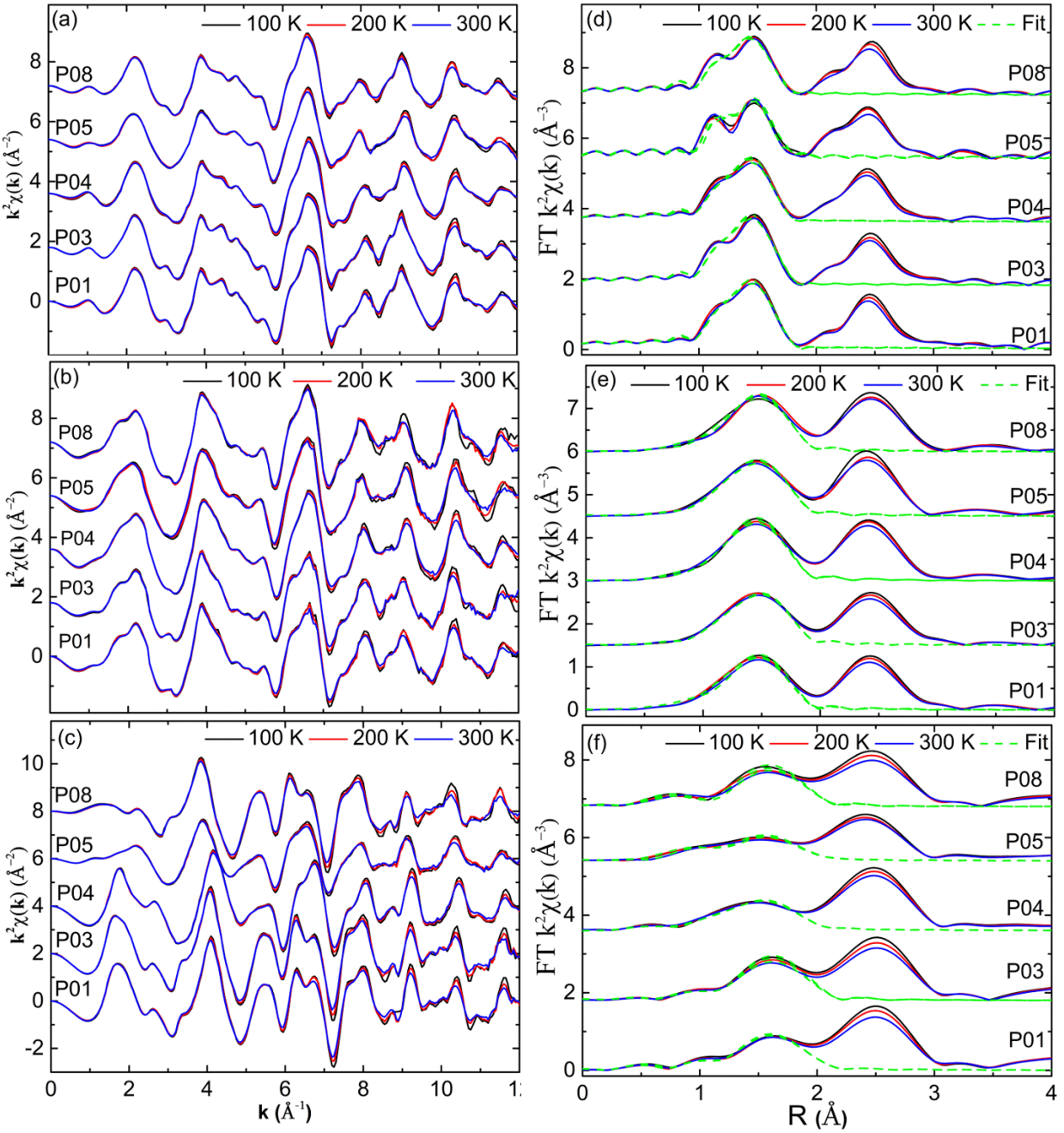

Figure S2. (a-c) Mn, Co, and Ni K-edge $k^2\chi(k)$ EXAFS oscillations and (d-f) the corresponding Fourier transform magnitudes, collected in the temperature range from 80 to 300 K over samples representing mainly the first charge/discharge cycle (solid lines). The dashed lines report the fits obtained for the first shell, with the points P01 (pristine), P03 and P04 (beginning and end of the voltage plateau), P05 (fully charged), and P08 (fully discharged after the first cycle) [s1].

The used EXAFS model for Mn considers the pristine sample to be consisting of two components: the layered $Li(Li_{0.2}Ni_xMn_yCo_z)O_2$ and the monoclinic Li_2MnO_3-like superlattice, which mixture corresponds to an averaged layered structure. During charge, the partial structural degradation of a unique averaged layered phase ($R\bar{3}m$ plus C2/m) into the spinel phase ($Fd\bar{3}m$) was investigated [s1- s4]. The phase coexistence need to be treated carefully, because the length of the spectrum limits the maximum number of free parameters for the EXAFS fitting (N_{ind}), and the window in the FT considered. Indeed, N_{ind} is given by the Nyquist theorem [s5]:

$$N_{ind} = \frac{2\Delta k \Delta R}{\pi} \qquad (2)$$

where Δk and ΔR are the windows used for the fittings.

Due to the limited number of free parameters, we implemented two different approaches in the analysis: (i) the analysis based on the ab initio real-space multiple scattering theory was done using the FEFF8 [s6, s7] and FEFFIT [s8] codes. Calculations of the scattering amplitude and phase shift functions were performed by the FEFF8 code, centered on the Mn, Ni or Co atom, and having a radius of 6 Å. The fitting of the experimental spectra was performed in the Fourier-transformed R space by the FEFFIT code. (ii) The semi-empirical approach [s9, s10], where the Mn backscattering amplitude and phase shift functions of each coordination shell were extracted experimentally from the pristine spectra. The Mn EXAFS oscillations for the pristine sample (P01) were modeled by considering the phase shifts and amplitude empirically calculated from the experimental spectra. Instead, for the Co and Ni EXAFS oscillations and the formed spinel phase, the ab initio calculated single scattering contributions were considered. For each component (layered or spinel), N_i was fixed to the average values known from diffraction studies [s2, s11-s13]. E_0 was empirically chosen by fitting the pristine and spinel reference spectra and then fixed to -0.11 eV, 0.21 eV, -1.21 eV, or -1.65 eV for Ni, Co, Mn layered, and spinel phases, respectively. S_0^2 was chosen by fitting the lowest temperature for each charge state and then fixed during the temperature-dependent analysis. S_0^2 was found to be oscillating around 0.68 for Ni and 0.74 for Co and 0.95 for Mn.

The distances R_i and the corresponding DWF σ_i^2 of the layered and spinel phase as well as the ratio between the two phases (x) were the fit parameters in the Mn EXAFS fitting model. The TM-O (TM = Co, Ni) distances (R_i) and the corresponding DWF (σ_i^2) were the fit parameters in the Ni and Co models, keeping the correlations between the fitting parameters to a minimum in the least-squares fits. The number of free parameters was then kept always below the maximum number in both models ($N_{ind\ (Mn)} \approx 6.71$, $N_{ind\ (Co)} \approx 4.99$ and $N_{ind\ (Ni)} \approx 5.22$).

The Mn, Co, and Ni K-edge EXAFS fits provided details about the Mn-O, Co-O, and Ni-O interatomic distances (R) and their corresponding mean square relative displacements (MSRDs) (σ^2) as a function of temperature for $Li[Li_{0.2}Ni_{0.16}Mn_{0.56}Co_{0.08}]O_2$ along the first cycle, as shown in **Figure S3** for (a,c) the Mn layered and (b,d) the Mn spinel, and in **Figure S4** for (a,c) the Co and (b,d) the Ni layered phases. The Mn-O, Co-O, and Ni-O distances in the layered structure (**Figure S3a** and **Figure S4a,c**) tend to contract during the first charge, which is consistent with earlier studies [s2, s3]. Regarding the spinel phase (**Figure S3c**), its local Mn-O bonding distance (R_{spinel}) shows a significant increase upon the first charge, followed by a reduction during the subsequent discharge [s3]. There is a small temperature effect due to the thermal expansion, which appears different for different states-of-charge, although the differences are within the experimental uncertainty.

The DWF (σ_i^2) covers the temperature-independent structural disorder effects (σ_0^2) as well as the thermal disorder (σ^2 (T)): i.e., $\sigma_i^2 = \sigma_0^2 + \sigma^2$ (T). A correlated Einstein model was used to describe the σ^2 (T) measured by EXAFS experiments [s5]. Indeed, in the harmonic and single scattering approximation, it is the simplest model to describe the temperature dependence of σ^2 (T). The used Einstein equation is:

$$\sigma^2(T) = \frac{\hbar^2}{2\mu k_B \theta_E} \coth\left(\frac{\theta_E}{2T}\right) \qquad (1)$$

where $\hbar$ is the Planck constant, μ is the reduced mass, k_B is the Boltzmann constant, T is the temperature, and θ_E is the Einstein temperature. The temperature-independent part of the correlated DWFs (σ_0^2, i.e., the static disorder) can be estimated by extrapolating the temperature behavior to 0 K (Fig 2c). The static disorder σ_0^2 of the Mn-O, Co-O, and Ni-O bonds tends to increase during the charge process. From the Einstein temperature, we have extracted the Einstein frequency

($\omega_E = k_B\theta_E/\hbar$) and quantified the effective local force constant ($K = \mu\omega_E^2$) for the Mn−O, Co−O, and Ni−O pairs (Fig 2d). The Einstein temperatures are included in **Table S1**.

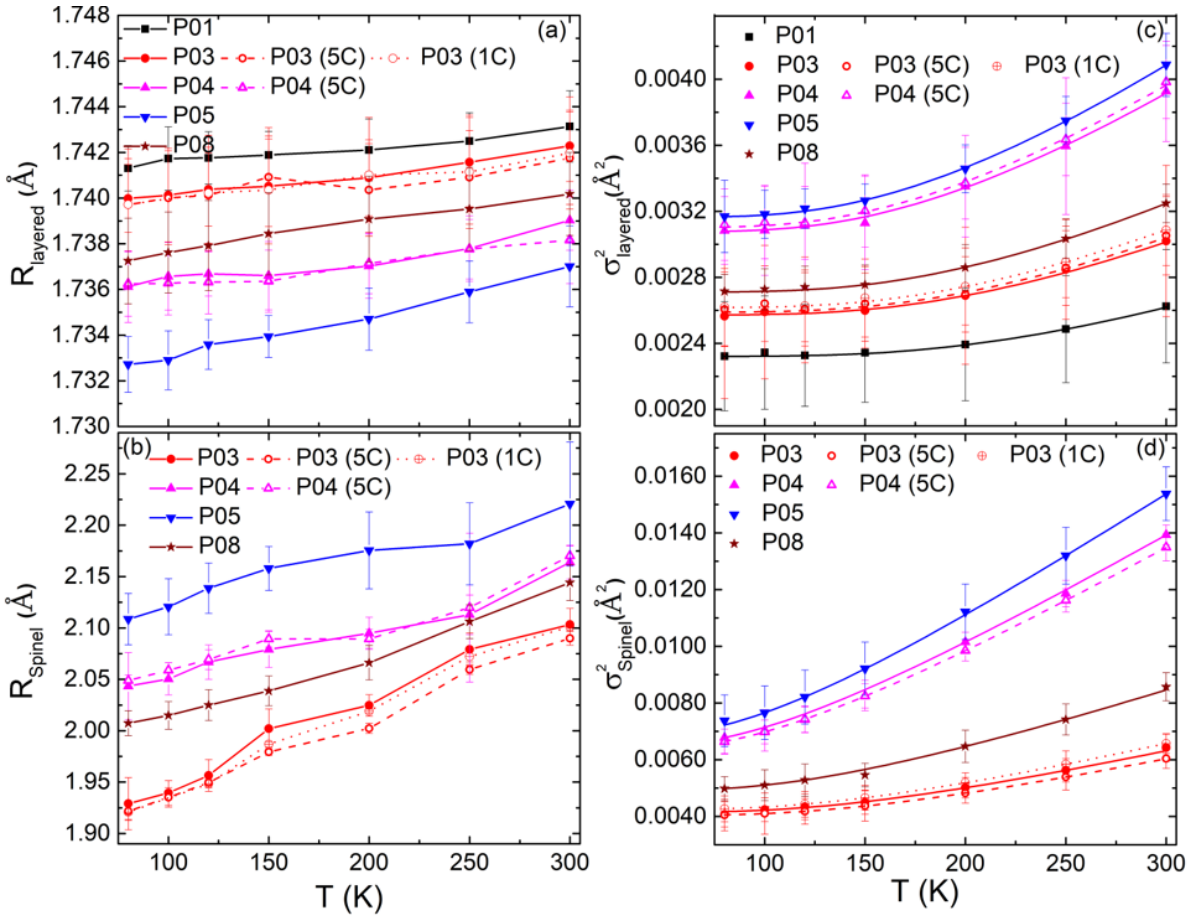

Figure S3. (a,b) The Mn−O bond lengths and (c,d) the temperature-dependent DWFs (σ^2) as a function of temperature for Mn in the layered structure (top panels) and Mn in the spinel structure (bottom panels) at different charge rates, i.e., 0.1C (solid lines), 1C (dotted lines), and 5C (dashed lines). The lines in the left panels represent the correlated Einstein model fits, 0.1C (solid lines), 1C (dotted lines), and 5C (dashed lines).

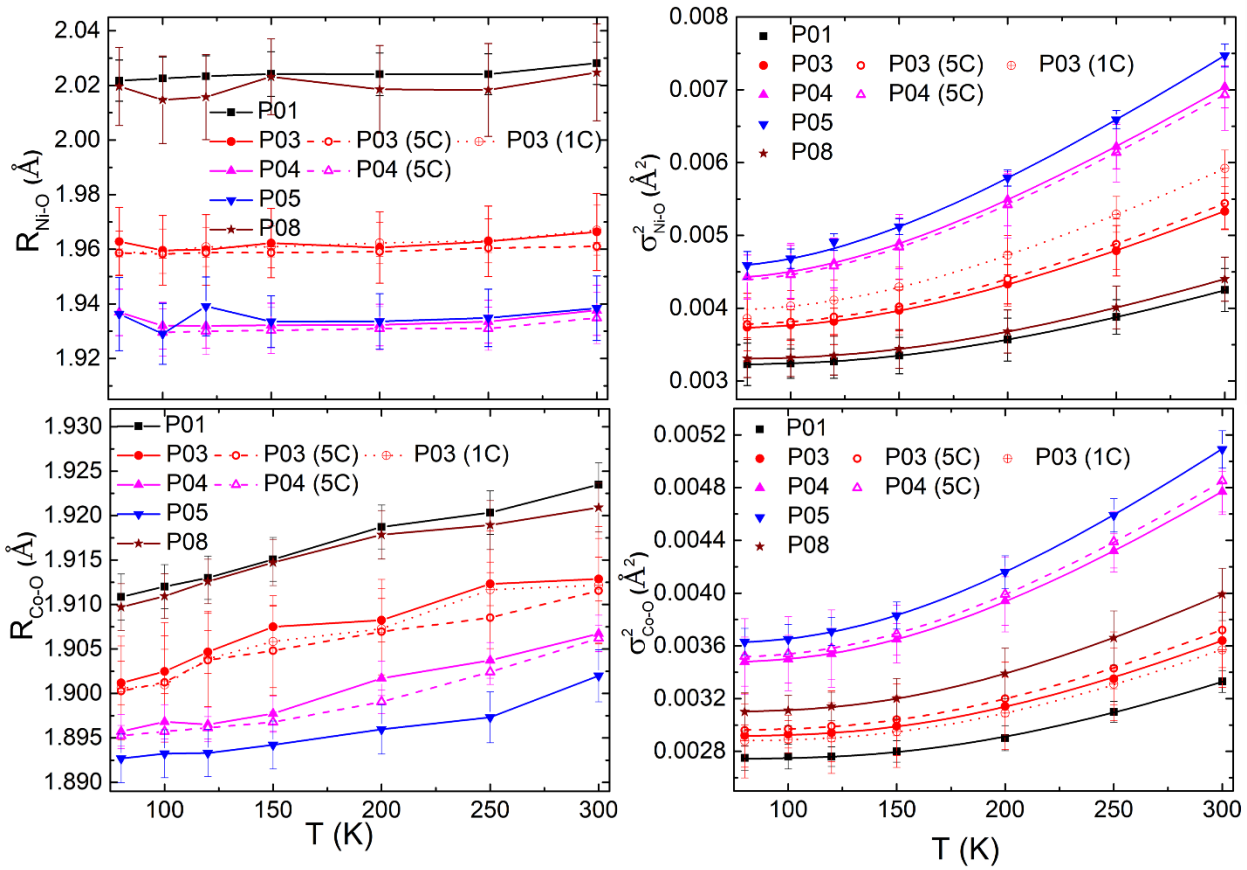

Figure S4. (a,b) The Co−O and Ni−O bond lengths and (c,d) the temperature-dependent DWFs (σ^2) as a function of temperature for Co (top panels) and Ni (bottom panels) at different charge rates, i.e., 0.1C (solid lines), 1C (dotted lines), and 5C (dashed lines). The solid lines in the left panels represent the correlated Einstein model fits, 0.1C (solid lines), 1C (dotted lines), and 5C (dashed lines).

Table S1. Einstein Temperatures (θ_E) for $Li[Li_{0.2}Ni_{0.16}Mn_{0.56}Co_{0.08}]O_2$ at the different states of charge.

Sample	Layered			Spinel
	Mn-O	Co-O	Ni-O	Mn-O
P01	843±42	703±67	598±35	-
P03	761±34	661±46	518±34	472±24
P04	636±32	555±31	439±34	302±18
P05	619±31	533±34	424±23	287±19
P08	722±40	622±36	584±31	398±22

Charge balance evaluation

We calculated the stoichiometry and redox states for the different samples using data quantified for Mn, Co, and Ni from the XAS measurements and electrochemistry, and imposing charge neutralityand some additional assumptions for the oxygen stoichiometry as detailed below. The lithium stoichiometry was calculated from the capacity Q, considering that 1.2*F electrons are released when lithium is completely extracted from 1 mol of the active material $Li_{1.2}Mn_{0.56}Ni_{0.16}Co_{0.08}O_2$:

$$x = 1.2*(1-Q/Q_{th}),$$
$$Q_{th} = (1.2*F) / M_w \quad mAh\ g^{-1}$$

where F is the Faraday constant (26,801.4 mAh mol^{-1}) and M_w the molecular weight (85.2 g mol^{-1}). The oxidation states of Mn, Co, and Ni were determined via XAS. In **Table S2**, we report the values obtained for the different samples at 0.1C and 5C.

Table S2. The oxidation states of Mn, Co, and Ni as well as the Li stoichiometry at 0.1C and 5C.

Sample	**Q (mAh g^{-1})**	**Li stoichiometry**	**Mn ox. State**	**Co ox. State**	**Ni ox. state**
P01 (0.1C)	0	1.200	+ 3.979	+3.000	+2.000
P03 (0.1C)	103	0.873	+ 3.861	+ 3.494	+3.268
P04 (0.1C)	200	0.565	+ 3.839	+3. 779	+4.000
P05 (0.1C)	347	0.098	+ 3.844	+3.975	+4.000
P08 (0.1C)	109	0.854	+ 3.884	+3.120	+2.068
P03 (5C)	98	0.873	+ 3.851	+ 3.555	+3.439
P04 (5C)	160	0.565	+ 3.785	+3. 803	+4.000

For oxygen, oxygen vacancies were considered in the pristine active material (P01) to compensate the Mn oxidation state, admitting O at the -2 state. The same assumption was made for the fully discharged sample (P08). No oxygen loss is assumed until P04, while the oxygen content in P05 is assumed equal to P08, implying loss at the end of charge (P04 → P05) in agreement with the literature [s15, s16]. Results are depicted in **Table S3**.

Table S3. The oxygen parameters for the two different dis-/charge rates of 0.1C and 5C.

Sample	**O stoichiometry**	**O ox. State**
P01 (0.1C)	1.994	-2.000
P03 (0.1C)	1.994	-1.924
P04 (0.1C)	1.994	-1.834
P05 (0.1C)	1.805	-1.777
P08 (0.1C)	1.805	-2.000
P03 (5C)	1.994	-1.938
P04 (5C)	1.805	-1.883

References

(s1) Simonelli, L.; Sorrentino, A.; Marini, C.; Ramanan, N.; Heinis, D.; Olszewski, W.; Mullaliu, A.; Birrozzi, A.; Laszczynski, N.; Giorgetti, M.; Passerini, S.; Tonti, D. Role of Manganese in Lithium- and ManganeseRich Layered Oxides Cathodes. J. Phys. Chem. Lett. **2019**, 10 (12), 3359-3368.

(s2) Buchholz, D.; Li, J.; Passerini, S.; Aquilanti, G.; Wang, D.; Giorgetti, M. X-ray Absorption Spectroscopy Investigation of Lithium- Rich, Cobalt-Poor Layered-Oxide Cathode Material with High Capacity. ChemElectroChem. **2015**, 2, 85.

(s3) Ali, S.; Olszewski, W.; Sorrentino, A.; Marini, C.; Kazzazi, A.; Laszczynski, N.; Birrozzi, A.; Mullaliu, A.; Passerini, S.; Tonti, D; Simonelli, L. Local interactions governing the performances of lithium- and manganese-rich cathodes, J. Phys. Chem. Lett. **2021**, 12 (4), 1195-1201

(s4) Sathiya, M.; Abakumov, A. M.; Foix, D.; Rousse, G.; Ramesha, K.; Saubanère, M.; Doublet, M. L.; Vezin, H.; Laisa, C. P.; Prakash, A. S.; Gonbeau, D.; VanTendeloo, G.; Tarascon, J. M. Origin of voltage decay in high-capacity layered oxide electrodes. Nat. Mater. **2015**, 14, 230

(s5) Prins, R., Koningsberger, D. C., Eds. X-Ray Absorption: Principles, Applications, Techniques of EXAFS, SEXAFS, XANES; Wiley: New York, **1988**.

(s6) Ankudinov, A.; Ravel, B.; Rehr, J.; Conradson, S. Phys. Rev. B **1998**, 58, 7565.

(s7) Rehr, J.; Albers, R. Theoretical Approaches to X-ray Absorption Fine Structure. Rev. Mod. Phys. **2000**, 72, 621.

(s8) Newville, M. J. Synchrotron Radiat. **2001**,8, 322.

(s9) Bunker, G. Nucl. Inst. Methods, **1983**, 207:437.

(s10) Monti, F.; Fornasini, P.; Sanson, A. J. Synchr. Rad.,**2001**, 8,1214.

(s11) Ohzuku, T.; Makimura, Y. Layered Lithium Insertion Material of $LiCo_{1/3}Ni_{1/3}Mn_{1/3}O_2$ for Lithium-Ion Batteries. Chem. Lett. **2001**, 30, 642.

(s12) Liu, Z. L.; Yu, A. S.; Lee, J. Y. Synthesis and Characterization of $LiNi_{1-x-y}Co_xMn_yO_2$ as the Cathode Materials of Secondary Lithium Batteries. J. Power Sources **1999**, 81, 416.

(s13) Sun, Y. K.; Kim, M. H.; Shin, H. S.; Shin, D. Synthesis and Electrochemical Properties of Li $[Ni_{0.8}Co_{0.1}Mn_{0.1}]$ O_2 and Li $[Ni_{0.8}Co_{0.2}]$ O_2 Via Co-Precipitation. J. Power Sources **2006**, 159, 1328.

(s14) Sevillano, E.; Meuth, H.; Rehr, J. J. Extended X-Ray Absorption Fine Structure Debye-Waller Factors. I. Monatomic Crystals. Phys. Rev. B: Condens. Matter Mater. Phys. **1979**, 20, 4908−4911.

(s15) Laszczynski, N.; von Zamory, J.; Kalhoff, J.; Loeffler, N.; Chakravadhanula, V. S. K.; Passerini, S. Improved Performance of VO_x-Coated Li-Rich NMC Electrodes. ChemElectroChem. **2015**, 2, 1768

(s16) Luo, K.; Roberts, M. R.; Hao, R.; Guerrini, N.; Pickup, D. M.;Liu, Y.-S.; Edström, K.; Guo, J.; Chadwick, A. V.; Duda, L. C.; *et al*. Charge-Compensation in 3d-Transition-Metal-Oxide Intercalation Cathodes through the Generation of Localized Electron Holes on Oxygen.Nat. Chem.**2016**,8(7), 684.